

Determining the radial pair distribution function from X-ray absorption spectra by use of the Landweber iteration method

André Rossberg^{a,b*} and Harald Funke^{a,b}

^aForschungszentrum Dresden-Rossendorf, Institute of Radiochemistry, Germany, and

^bThe Rossendorf Beamline at ESRF, France. E-mail: rossberg@esrf.fr

Received 29 June 2009

Accepted 4 December 2009

The Landweber iteration approach is used to construct the radial pair distribution function (RPDF) from an X-ray absorption (EXAFS) spectrum. The physical motivation for the presented investigation is the possibility to also reconstruct asymmetric RPDFs from the EXAFS spectra. From the methodical point of view the shell fit analysis in the case of complicated spectra would be much more eased if the RPDF for the first shell(s) are computed precisely and independently. The RPDF, as a solution of the fundamental EXAFS integral equation, is examined for theoretical examples, and a detailed noise analysis is performed. As a real example the EXAFS spectrum of curium(III) hydrate is evaluated in a stable way without supplementary conditions by the proposed iteration, *i.e.* by a recursive application of the EXAFS kernel.

© 2010 International Union of Crystallography
Printed in Singapore – all rights reserved

Keywords: EXAFS; pair distribution function; Fredholm integral equation; Landweber iteration.

1. Introduction

The atomic pair distribution function describes the density of interatomic distances in matter. The radial pair distribution function (RPDF), which is independent of orientation, is of special practical importance for the analysis of EXAFS spectra. It is a major descriptor for the atomic structure of amorphous materials and liquids.

A RPDF has by definition the following properties (Babanov *et al.*, 1981):

- (i) $g(r) \geq 0$ for any r ,
- (ii) $g(r) \rightarrow 1$ if $r \rightarrow \infty$,
- (iii) $g(r) \rightarrow 0$ if $r \rightarrow r_{\min}$, $g(r) = 0$ if $r < r_{\min}$, (1)
- (iv) $(1/V) \int_0^{\infty} 4\pi r^2 g(r) dr = 1$.

The first condition is the positivity constraint, which is valid for each probability distribution. The second condition states that, for large distances where the particles are uncorrelated, $g(r)$ tends to 1.† Thirdly, for distances smaller than the sum of ionic radii of the two atoms (r_{\min}), where the impenetrability of the particles becomes apparent, $g(r)$ is equal to zero. Fourthly, $g(r)$ is normalized to 1.

† This boundary condition is irrelevant for RPDFs, which are derived from EXAFS measurements. The distance of neighboring atoms measured by EXAFS spectra is smaller than the asymptotic value of r , for which $g(r) \rightarrow 1$ is valid.

The conditions in (1) must be incorporated in the construction procedure of the function $g(r)$, thus ensuring that the sought solution is a normalized RPDF.

The general EXAFS integral equation for a one-component system, *i.e.* for a system with only one type of backscattering atoms, has the form

$$\chi(k) = \int_{R^3} \frac{F(k, r)}{kr^3} \exp\left[-\frac{2r}{\lambda(k)}\right] \times \sin[2kr + 2\delta(k) + \varphi(k, r)] g(r) dV, \quad (2)$$

where the kernel

$$A(k, r) = \frac{F(k, r)}{kr^2} \exp\left[-\frac{2r}{\lambda(k)}\right] \times \sin[2kr + 2\delta(k) + \varphi(k, r)] \quad (3)$$

results from the matrix element of the electron scattering according to Fermi's Golden Rule (see Stern, 1974; Lee & Pendry, 1975; Teo, 1986). Here $\chi(k)$ is the normalized oscillating part of the measured EXAFS spectrum, k is the electron wavevector, and r is the distance from the central to the backscattering atoms. The function's backscattering amplitude $F(k, r)$, the central atom phase shift $\delta(k)$, the backscattering atom phase shift $\varphi(k, r)$ and the mean free path of the photoelectron $\lambda(k)$ are obtained from the curved wave approximation using the *FEFF* code (Ankudinov *et al.*, 1998). The reduction factor is set to $S_0^2 = 1$ in this article.

Equation (2) may be simplified in spherical coordinates due to the fact that the kernel depends only on the radius r . In this case the volume element is $dV = 4\pi r^2 dr$. For EXAFS data analysis it is more demonstrative and more adapted to introduce a radial particle distribution $n(r)$ instead of $g(r)$,

$$n(r) = 4\pi r^2 g(r), \quad (4)$$

with

$$N = \int_{r_1}^{r_2} n(r) dr, \quad (5)$$

so that N is the number of backscattering atoms in the spherical shell between r_1 and r_2 , *i.e.* the analogue to the coordination number.

The EXAFS equation (2) now takes the form

$$\chi(k) = \int_0^\infty \frac{F(k, r)}{kr^2} \exp\left[-\frac{2r}{\lambda(k)}\right] \times \sin[2kr + 2\delta(k) + \varphi(k, r)] n(r) dr. \quad (6)$$

The function $n(r)$, depending on the radius, is unknown and contains all the information about the EXAFS spectrum.

The ‘shell fitting’ procedure is the most frequently applied method to evaluate EXAFS spectra in practice. In this procedure it is usually assumed that the particle density is represented by separated Gaussian peaks where the half width of the Gauss curve is the Debye–Waller factor σ^2 ,

$$n(r) = \sum_{m=1}^{\text{shells}} \frac{N_m}{(2\pi\sigma_m)^{1/2}} \exp\left[-\frac{(r - r_m)^2}{2\sigma_m^2}\right]. \quad (7)$$

Thus, the integral in the EXAFS equation (6) can be resolved analytically and, assuming some well justified approximations, will be reduced to the EXAFS equation for a number of coordination shells,

$$\chi(k) = \sum_{m=1}^{\text{shells}} \frac{N_m F_m(k, r_m)}{r_m^2 k} \exp\left[-\frac{2r_m}{\lambda(k)}\right] \exp(-2\sigma_m^2 k^2) \times \sin[2kr_m + 2\delta(k) + \varphi(k, r_m)]. \quad (8)$$

Here, N_m is the coordination number and σ_m^2 is the Debye–Waller factor of the backscattering atoms in the m th shell.

While the shell fitting procedure approximates $n(r)$ by symmetrical Gaussians, knowledge of the exact RPDF, or equivalent $n(r)$, is of greatest importance, *e.g.* for the investigation of anharmonic corrections caused by thermal vibrations (Yang & Joo, 1998; Dalba & Fornasini, 1997; Crozier *et al.*, 1988). This is the main physical reason to determine the complete RPDF independently.

Equation (6) may be rewritten in a condensed form as

$$\chi(k) = \int_0^\infty A(k, r) n(r) dr. \quad (9)$$

This is a Fredholm integral equation of the first type connecting the known spectrum $\chi(k)$ with the unknown function $n(r)$. The inversion of equation (9), *i.e.* the determination of $n(r)$, is a so-called ill-posed problem. From the three conditions for a well posed problem, suggested by Hadamard

(1932), *i.e.* (i) the existence, (ii) the uniqueness and (iii) the stability of the solution depending continuously on the data, condition (iii) is most often violated owing to the uncertainties in the data, *i.e.* experimental error. The two most important well established methods for the solution of this type of integral equations, like equation (9), are Tikhonov’s regularization (Tikhonov & Arsenin, 1981) and Landweber’s iteration (Landweber, 1951) procedures. The principal difference between the methods is the following. The integral equation, like equation (9) or (10), is solved using the Tikhonov regularization by multiplication with the inverse matrix (*i.e.* the inverse integral operator), whose irregularities are avoided by addition of a regularization matrix. The Landweber iteration (see details below) does not use the inverse matrix and therefore does not contain irregularities. Both methods are independent and different.

In the mathematical literature some comparisons of the two methods exist (Kirsch, 1996; Latham, 1998). They stated that for non-noisy model spectra both methods lead to the same result. A general comparison of both methods for the case of realistic noisy data is not possible because of the different character of data errors for each individual case.

It has been confirmed that for the inversion of equation (9), and for data with experimental error, more stable results are supplied by the Landweber iteration (Kirsch, 1996), which on the other hand needs more iteration steps. The latter statement agrees with our initial experiences of the analysis of EXAFS spectra using the Landweber iteration. However, no direct comparison of both methods, applied to real noisy EXAFS spectra, exists. In §3 a qualitative noise analysis for the Landweber iteration using model spectra is presented.

Babanov and co-workers (Babanov *et al.*, 1981, 2007; Ershov *et al.*, 1981; Kunicke *et al.*, 2005; see also Yang & Bunker, 1996; Khelashvili & Bunker, 1999; Bunker *et al.*, 2005; Ageev *et al.*, 2007) have applied the Tikhonov regularization to the analysis of EXAFS spectra. Using special assumptions, adequate RPDF of various systems were reconstructed. In this context no systematic noise analysis exists.

Lee & Yang (2006) presented a new analytical method, the Matched EXAFS RPDF Projection (MEPP), to obtain the RPDF of an EXAFS spectrum *via* Fourier filtering.

An interesting article by Yamaguchi *et al.* (1999) deals with the application of the Landweber iteration to the inversion of the EXAFS equation. Their work focuses on the application of the wavelet Galerkin method for the reconstruction of the integral kernel $A(k, r)$ in equation (9). The Landweber iteration method contains two parameters (see below): a convergence parameter α and a stopping number ν_{opt} , which indicates the optimal number of iterations. Both parameters were set by Yamaguchi *et al.* (1999) by ‘trial and error’ to 5000.

In the present work we present a methodical introduction and some examples for the analysis of EXAFS spectra using the Landweber iteration method, including the convergence parameter α , which depends on the norm $\|A^* A\|^\dagger$, and the

† A^* denotes the conjugate transpose. Here and in the following the norm of a matrix is the Frobenius norm.

stopping parameter ν_{opt} , which depends on the error in the data. The calculation of the matrix A is performed by the use of the *FEFF8.2* program (Ankudinov *et al.*, 1998). We also give a physical interpretation of the iteration steps of the Landweber method for the inversion of the EXAFS equation. In favor of simplicity and clarity, the article does not contain analysis of multi-component spectra and of multiple scattering effects.

2. Landweber's iteration for a one-component backscattering system without multiple scattering effects

2.1. Landweber's iteration and constraints

2.1.1. Definition. The basic EXAFS equation (6), in operator form

$$An = \chi, \quad (10)$$

when multiplied by αA^* , is identically rewritten as

$$n = (I - \alpha A^* A)n + \alpha A^* \chi. \quad (11)$$

Based on this equation, with initial condition $n_0 = 0$ and a parameter $\alpha > 0$, Landweber (1951) suggested the iteration scheme

$$n_{\nu+1} = n_\nu + \alpha A^*(\chi - An_\nu), \quad (12)$$

where ν is the iteration number. For mathematical details, see for example the textbooks by Kirsch (1996) and Louis (1989). This iteration procedure can be interpreted as the steepest descent algorithm to minimize the functional $\|An - \chi\|$ with α as convergence parameter. We remark that the acceleration term $(\chi - An_\nu)$ is the difference spectrum between the original spectrum χ and the last iteration spectrum An_ν .

2.1.2. Convergence parameter. It has been proven, *e.g.* by Louis (1989), that for α in the range $0 < \alpha < 2/\|A^*A\|$, the Landweber algorithm is equivalent to a linear regularization procedure. This means that the iteration converges to an optimal solution $n_{\nu_{\text{opt}}}$ at an optimal number of iterations ν_{opt} . In the following examples, the convergence parameter $\alpha^{\text{EXAFS}} = 1/\|A^*A\|$ will be chosen.

2.1.3. Stopping parameter. While α defines only the 'speed' of the iteration, the optimal stopping parameter ν_{opt} must be defined for each problem separately. On one hand, iterating too long causes the experimental error in the data to increasingly disturb the solution. On the other hand, too few iterations will lead to a loss of resolution. This convergence behavior is called semi-convergence (see also Fig. 1a).

Apparently, the stopping parameter ν_{opt} depends on the error in the data (δ), *e.g.* caused by noise, spline errors *etc.* All other sources of uncertainty, *e.g.* the choice of α and the model matrix A , are described in the literature (Elfving & Nikazad, 2007; Kirsch, 1996) by an additional parameter τ . There, it is proved that the iterative method is convergent for $0 < \tau < 2$. Our initial model calculations (see below) show best results for $\tau \simeq 1$.

If the total data error $\tau\delta$ were known, the stopping rule defining ν_{opt} would simply be

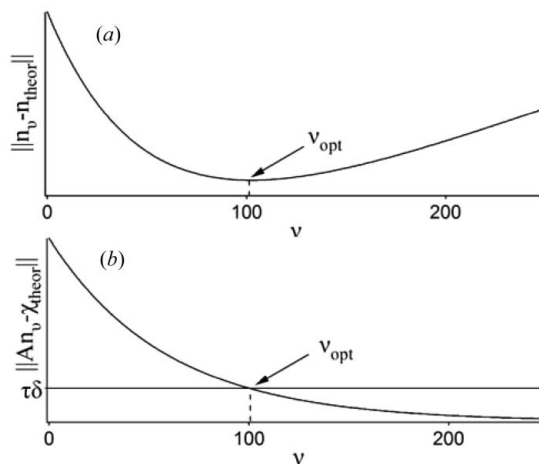


Figure 1 Definition of the stopping parameter for an idealized theoretical spectrum which contains artificial data error. (a) The difference between the iterated (n_ν) and the theoretical (n_{theor}) RPFD, demonstrating clearly the semi-convergent behavior of the Landweber iteration. (b) The difference between the iterated and the theoretical spectrum plotted over the iteration parameter ν . $\tau\delta$ is the total error.

$$\text{if } \|An_\nu - \chi\| \leq \tau\delta: \nu = \nu_{\text{opt}}. \quad (13)$$

This means that the solution is such that the norm of the residual $\|An - \chi\|$ is of the same order as the total data error $\tau\delta$ (Fig. 1b). We have used this condition several times with simulated noise, *i.e.* with known δ and $\tau \simeq 1$, to validate the following procedure developed for realistic noisy data.

2.1.4. L-curve criterion. In the case of real EXAFS measurements, the total error $\tau\delta$ is not known. To determine the stopping parameter in the Landweber iteration we adapted the concept of the L-curve criterion, derived for the determination of an optimized regularization parameter for the Tikhonov regularization (Hansen, 1992, 2001; Hansen & O'Leary, 1993; Kunicke *et al.*, 2005). In general, the L-curve is a log-log plot of the norm of a regularized solution *versus* the norm of the corresponding residual. Both norms depend parametrically on ν_{opt} . The resulting curve shows a shape like the capital letter L (Fig. 2). The optimal regularization parameter is chosen as the maximum of the L-curve curvature, corresponding to the corner of the L. As ν increases up to the

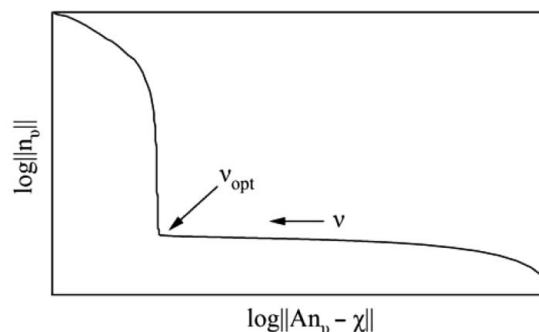


Figure 2 A typical idealized L-curve. The function n_ν is the RPFD after the ν th iteration, χ is the measured EXAFS spectrum, and A is the EXAFS integral operator. The iteration number ν increases from right to left.

value ν_{opt} , the norm of the residual decreases much faster than the norm of the solution increases. A region of ν values follows where the norm of the solution starts to increase dramatically. This means that the value ν_{opt} , corresponding to the corner of the L-curve, gives an optimum in the effort to minimize simultaneously the norm of the residual and the norm of the solution.

In the ideal case the L-curve is defined by a smooth computable formula. Then the maximum of the curvature of the graph $\log\|n_\nu\|$ over $\log\|An_\nu - \chi\|$ gives us the value of ν_{opt} .

The curvature c_ν of the L-curve is obtained using equation (14) where $x = \log\|An_\nu - \chi\|$ and $y = \log\|n_\nu\|$. The prime denotes the derivative with respect to ν if both functions depend parametrically and continuously on the parameter ν ,

$$c_\nu = \frac{x'y'' - y'x''}{(x'^2 + y'^2)^{3/2}}. \quad (14)$$

Unfortunately, in the case of realistic data the L-curve does not have the clear form shown in Fig. 2, and is limited by the knowledge of only a finite set of points. As a first approximation for the numerical differentiations in equation (14) we used the integral values of the parameter ν as nodes. The corresponding stopping parameter is further denoted by ν_{curv} . The use of ν_{curv} resulted in satisfying curvature maxima for all of our examples.

A complete discussion of the numerical problems in locating the corner of the L-curve, e.g. by use of cubic spline curves, is given by Hansen & Oleary (1993).

2.1.5. Positivity constraint. Generally, different constraints are used for the construction of solutions of ill-posed problems in order to improve their stability and convergence. A common method is the utilization of positivity constraints (Kirsch, 1996). The positivity constraint [see equation (1)] is included in the Landweber iteration steps because it is an inherent part of the definition of the RPDF. It should be noted that the consideration of the positivity constraint leads to a slight degradation of the smoothness of the L-curve. Instead of the terminus ‘positivity constraint’ the terminus ‘projected inversion’ is equivalently used in the relevant literature (Bunker, 2009).

2.2. Physical interpretation of the transformation of the spectrum by the transposed matrix A^*

In the first step of the Landweber iteration ($n_0 = 0$) and with $\alpha = 1$, equation (12) has the form $n_1 = A^*\chi$, where χ is the EXAFS spectrum. In each further iteration step the operator A^* acts on a difference of two EXAFS spectra ($\chi - An_\nu$). We consider the effect of the transposed matrix A^* acting on the spectrum $\chi(k)$,[†]

$$A^*\chi \equiv A_{ni}\chi_i \equiv \sum_i A(k_i, r_n)\chi_i, \quad (15)$$

and rewrite (15) according to (6) in its continuous form,

[†] For the discretization of the EXAFS equation (6) we use the following. The indices i, j, \dots run from 1 to the maximum number $i_{\text{max}}, j_{\text{max}}$ etc. of points in k -space. The indices m, n, \dots run from 1 to the maximum number $m_{\text{max}}, n_{\text{max}}$ etc. of points in r -space.

$$(A^*\chi)(r) = \int_0^\infty \frac{F(k, r)}{kr^2} \exp\left[-\frac{2r}{\lambda(k)}\right] \times \sin[2kr + 2\delta(k) + \varphi(k, r)]\chi(k) dk, \quad (16)$$

from which the following interpretation of transformation (16) is obvious. The oscillating part of the integration kernel, $\sin(2kr)$, is the imaginary part of the Fourier transform, which results usually in a very precise determination of the distances of the backscattering atoms. The argument of the sine function is phase corrected by the phases of the central and backscattering atoms, and an amplitude window function is formed by the atomic amplitudes and the mean free paths. Therefore the transform (16) may be interpreted as a windowed and phase-corrected Fourier transform, whereas the window and phase functions originate from the underlying model.

2.3. Construction of the matrix A

For the discretization of equation (6) by an equal-spaced step function, $n(r_m)$ is approximated by a linear function in each Δr interval.

Consequently, the right-hand side of (8) represents the columns of the matrix A_{im} , which correspond to the k -dependence of the kernel for each distance r_m . If the coordination number in each interval is set to $N_m = 1$, we obtain the columns of A_{im} ,

$$\chi^{[r_m]}(k) = \frac{1}{r_m^2} \frac{F(k, r_m)}{k} \exp\left[-\frac{2r_m}{\lambda(k)}\right] \times \sin[2kr_m + 2\delta(k) + \varphi(k, r_m)]. \quad (17)$$

Therefore, for the distances r_m , the columns of A_{im} are calculated directly from the *FEFF* program (the *chi.dat* files without Debye–Waller factors) in the form of the theoretical $\chi^{[r_m]}(k)$ spectra. We used step sizes of $\Delta r = 0.02 \text{ \AA}$ or $\Delta r = 0.002 \text{ \AA}$ in our calculations.

Most algorithms use for the description of an RPDF peak the theoretical scattering functions calculated for one radial distance supplied by the *FEFF* structural model. It is well known that the theoretical scattering functions depend on the radial distance. Therefore the theoretical scattering functions must be calculated for a narrow grid of radial distances in the r -interval of the RPDF. If the theoretical scattering functions are calculated only for one radial distance then, especially for strong disordered systems with a broad RPDF, the calculated RPDF might be incorrect.

2.4. Determination of the energy threshold shift ΔE_0

The k -axis, which is the basis for the computation of the matrix A , is defined by

$$k = \left[(2m/\hbar^2)(E - E_0 + \Delta E_0)\right]^{1/2}, \quad (18)$$

where \hbar is Planck’s constant, m is the electron mass and E is the photon energy. E_0 is the threshold energy, i.e. the minimum energy to free the electron. To define the k -axis of the real experiment, usually a correction term ΔE_0 is introduced. ΔE_0 is *a priori* unknown and usually it is determined by a shell fit

of the spectrum before an inversion method is applied. If the shell fit model is incorrect then the determined ΔE_0 is erroneous and an inverse method would give a wrong RPDF. This leads in turn to the conclusion that the recent inversion procedures are only applicable if the structural model for the investigated system is already known.

In our approach, ΔE_0 is defined by the iteration procedure itself, without recourse to fit calculations or models. The only assumption is that for each ν an optimal ΔE_0 exists, and that over a broad range around ν_{opt} the best values of ΔE_0 are similar. By using this assumption for a given ν , the optimal ΔE_0 is determined simply by a one-parameter search, using the minimization of the standard deviation SD_ν , defined as

$$SD_\nu = \frac{\|An_\nu - \chi\|}{i_{max}^{1/2}} \quad (19)$$

SD_ν is the norm of the residual of the EXAFS equation (10), and depends on the iteration number ν , normalized to the maximum number of data points in r -space (i_{max}).

We start with arbitrarily chosen values ν_{start} and ΔE_0 . With this start energy threshold shift (e.g. $\Delta E_0 = 0$) the columns in the matrix A_{im} are re-calculated on the new k -axis, based on equation (18). Then the Landweber iteration is performed up to ν_{start} and the new SD_ν is determined. In the next cycle, ΔE_0 is modified so that SD_ν decreases. If ΔE_0 converges to a constant value, the approximation procedure based on ν_{start} is stopped. This first optimal ΔE_0 is already near the true value, and we calculate with this ΔE_0 the new L-curve and the new ν_{curv} . Then the algorithm to find ΔE_0 is repeated by using ν_{curv} as the new ν_{start} . If the actual ν_{start} is equal to the next ν_{curv} , then ΔE_0 and SD_ν have reached their final values.

This procedure will be illustrated below, where ΔE_0 is determined for the noise contaminated spectrum of example #6.

3. Application of Landweber's iteration to model spectra

In this section, we examine theoretically how the Landweber iteration method responds to noisy 'close-to-reality' spectra. Noise is added in ten steps with a noise generator to a noise-free theoretical spectrum (Table 1, example #1). Subsequently, the ten noise-contaminated spectra are analyzed. The change of the structural parameter (N, r, σ^2) and the stopping parameter are inspected as a function of the amplitude of the added noise.

Additionally, the difference between the theoretical stopping parameter ν_{theor} (equivalent to ν_{opt} in Fig. 1a) and the stopping parameter ν_{curv} (equivalent to ν_{opt} in Fig. 2), determined from the curvature of the L-curve, will be discussed.

By using equation (7) we calculated for one oxygen shell a Gaussian-shaped model RPDF (n_{theor}) with $N = 1, r = 2.50 \text{ \AA}$ and $\sigma^2 = 0.005 \text{ \AA}^2$. The terms in equation (8) [$F(k, r), \lambda(k), 2\delta(k)$ and $\varphi(k, r)$] are calculated by *FEFF8.20* (see §2.3), where the amplitude reduction factor is set to $S_0 = 1$. The *FEFF* structural model consists of a curium hydrate cluster based on

Table 1

Summary of the structural parameters N, r, σ^2 , the theoretical (ν_{theor}) and L-curve defined stopping parameter (ν_{curv}) for the noise-contaminated model spectra.

The sign ∞ for example #1 remarks that, for a spectrum without error, an *a priori* limitation rule for the iteration does not exist, as explained in §2.1.3. Standard deviations of the parameter are given in parentheses.

Example	$C_{noise} \times 10^4$	N	$r \text{ (\AA)}$	$\sigma^2 \times 10^3 \text{ (\AA}^2\text{)}$	ν_{theor}	ν_{curv}
#1	0.00	1	2.5	5	∞	∞
#2	0.50	0.999 (6)	2.5000 (5)	4.99 (7)	84	93
#3	0.75	0.995 (7)	2.4999 (6)	4.93 (8)	75	79
#4	1.00	0.991 (8)	2.4999 (6)	4.88 (9)	70	72
#5	1.50	0.98 (1)	2.4998 (8)	4.8 (1)	62	64
#6	2.00	0.98 (1)	2.500 (1)	4.7 (1)	57	59
#7	2.50	0.97 (1)	2.500 (1)	4.6 (2)	53	56
#8	3.00	0.97 (2)	2.499 (1)	4.5 (2)	50	55
#9	3.50	0.97 (2)	2.499 (2)	4.4 (2)	48	53
#10	4.00	0.96 (2)	2.499 (2)	4.3 (2)	46	51

the EXAFS results of Skanthakumar *et al.* (2007). The matrix A_{im} is then calculated using (17) with an energy shift of $\Delta E_0 = 5 \text{ eV}$ [see (18)] and the model spectrum χ is calculated using (10). For the calculation of the k -axis we used (18). We added to the unweighted spectrum χ a noise equal to $C_{noise} \cdot \text{rnd}$, where the random number generator (rnd) gives values in the range $-0.5 < \text{rnd} < 0.5$ (Table 1). Fig. 3 shows for examples #2, #6 and #10 (Table 1) the theoretical RPDF and the noise-contaminated spectra.

For examples #2–#10 the L-curves are shown in Fig. 4 with an inset showing example #10 on a more convenient scale. For the presented theoretical examples, n_{theor} is known, hence for each example the theoretical optimum number of iterations ν_{theor} can be determined as the minimum in $\|n_\nu - n_{theor}\|$ normalized to the maximum number of data points in r -space (m_{max}). Figs. 5(a) and 5(b) illustrate the determination of ν_{theor} and ν_{curv} for the examples #2–#10.

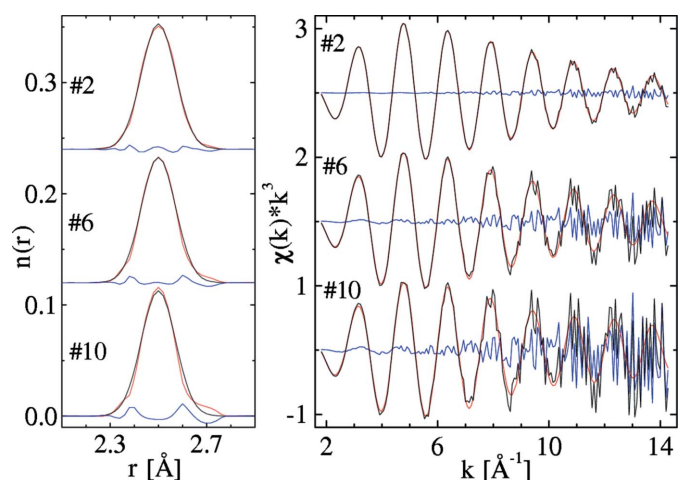


Figure 3

Theoretical RPDFs (n_{theor}) and the corresponding spectra with added artificial noise are shown in black. The RPDFs ($n_{\nu_{curv}}$) reconstructed using the Landweber iteration and the corresponding spectra are shown in red. Residuals are blue.

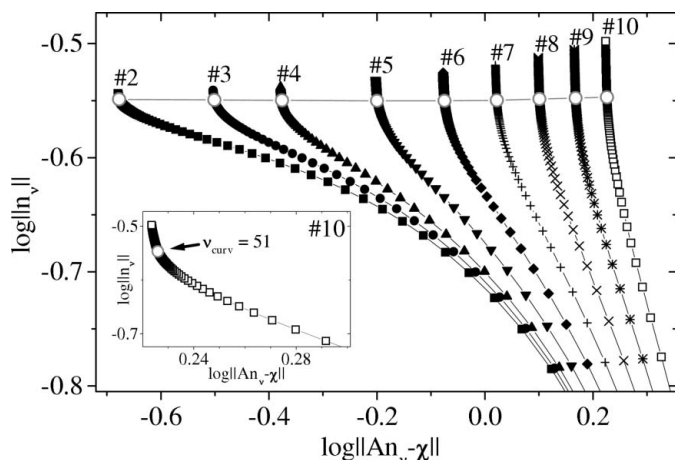


Figure 4
L-curves for the noise-contaminated spectra of examples #2–#10 (Table 1).

The inspection of the shape of the L-curves (Fig. 4) leads to the conclusion that for examples with a high noise level the norm of the residual $\|An_v - \chi\|$ decreases and the norm of the solution $\|n_v\|$ increases faster than for the examples with a lower noise level; hence the higher the experimental error in the data the lower is the number of iterations needed for the

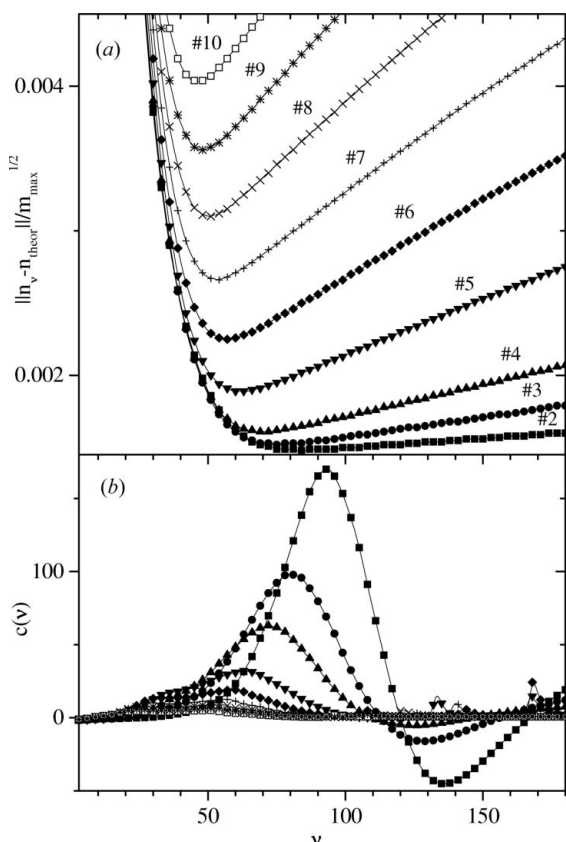


Figure 5
Definition of the stopping parameters ν_{theor} and ν_{curv} for the noise-contaminated spectra of examples #2–#10 (Table 1). (a) The difference between the theoretical and the iterated RPDF, normalized to the maximum number of data points in r -space. (b) The curvature [see equation (14)] of the L-curves (Fig. 4). For graphs (a) and (b) the symbols correspond to the numbers of the examples.

Table 2

Determination of ΔE_0 for the noisy spectrum of example #6, arbitrarily starting at $\nu_{\text{start}} = 10$ and $\nu_{\text{start}} = 100$.

Step	ν_{start}	ν_{curv}	ΔE_0 (eV)	$SD_\nu \times 10^2$ (\AA^{-3})
1	10	64	5.08	6.286
2	64	67	5.13	6.284
3	67	68	5.14	6.283
4	68	68	5.14	6.283
1	100	66	5.11	6.284
2	66	68	5.14	6.283
3	68	68	5.14	6.283

solution. This trend is in accordance with the shift of the minimum in $\|n_v - n_{\text{theor}}\|$ and $c(\nu)$ to smaller ν_{theor} and ν_{curv} , in case the noise level increases [Figs. 5(a) and 5(b)]. These observations are in line with the semi-convergent behavior of the Landweber iteration. The observed good accordance between ν_{curv} and ν_{theor} (Table 1) shows the reliability of the L-curve concept to estimate the number of required iterations for noise-contaminated spectra.

For all L-curves, the position of the maximum curvatures determined by equation (14) shows a very similar norm $\|n_v\|$ (open circles connected by line in Fig. 4). This is a first indication that for all calculated RPDFs the coordination number will be very similar as discussed later.

For all examples, the determined $n_{\nu_{\text{curv}}}$ and the theoretical n_{theor} are in good accordance, as can be seen for examples #2, #6 and #10 in Fig. 3. Also, the spectra calculated using $n_{\nu_{\text{curv}}}$ are in good agreement with the noise-contaminated spectra within the noise level (Fig. 3).

The sought structural data (N, r, σ^2) in Table 1 are derived from a comparison of the RPDFs with a Gaussian-shaped RPDF [see equation (7)]. For all noise levels the structural parameters (N, r) are in good agreement with those of the initial model (Table 1, #1). The deviation of σ^2 from its true value increases systematically and significantly with the noise level. For example #2, no significant deviation is observed, whereas, for example #10, σ^2 is 14% below the true value (Table 1). It is interesting to note that the precision in the determination of the structural parameters follows the order $r > N > \sigma^2$. This trend is also visible in the deviations between $n_{\nu_{\text{curv}}}$ and n_{theor} (Fig. 3). The position of the maxima in $n_{\nu_{\text{curv}}}$ does not change with the noise level, while the left- and right-hand sides of $n_{\nu_{\text{curv}}}$ show deviations from n_{theor} with increasing noise (Fig. 3). It is important to realise that these deviations influence the shape of the RPDF and that therefore σ^2 is the parameter which is most affected by noise, *i.e.* experimental error, of the EXAFS spectrum.

Note that for the preceding comparison of models the energy shift for the noise-free spectrum was fixed at $\Delta E_0 = 5$ eV. In the following we demonstrate, using example #6, the procedure for calculating ΔE_0 as described in §2.4. For this spectrum, $\nu_{\text{theor}} = 57$ and $\nu_{\text{curv}} = 59$ (Table 1, #6).

The starting values are $\nu_{\text{start}} = 10$ and $\Delta E_0 = 0$ eV. At $\nu_{\text{start}} = 10$ the resulting ΔE_0 is 5.08 eV (Table 2), hence already near the value of a noise-free initial spectrum (Table 1, #6). The curvature shows for this first value of ΔE_0 a maximum at

Table 3

Structural parameters for example #6 determined by the Landweber iteration including the calculation procedure of ΔE_0 and the structural parameters determined by shell fitting.

Standard deviations of the parameter are given in parentheses. In the case of the shell fit, the standard deviations were calculated by using the software EXAFSPAK (George & Pickering, 1995).

Example #6	N	r (Å)	σ^2 (Å ²)	ΔE_0 (eV)
Iteration	0.98 (1)	2.500 (1)	0.0047 (1)	5.14
Shell fit	0.96 (3)	2.494 (2)	0.0046 (2)	4.9 (3)

$\nu_{\text{curv}} = 64$ (Table 2). By taking this value as the next ν_{start} , a new improved ΔE_0 is determined. After four such steps, ν_{start} is equal to ν_{curv} and ΔE_0 has reached a final value of 5.14 eV. When starting at $\nu_{\text{start}} = 100$, the method leads to the same result (Table 2). During the approximation cycles the value of SD_ν decreases and the difference between the theoretical ($\Delta E_0 = 5$ eV) and the calculated ΔE_0 increases slightly. This demonstrates that a part of the noise in the spectrum influences ΔE_0 and consequently influences the RPDF, which reflects the normal behavior of error propagation.

Table 3 shows the structural parameters for example #6, determined either by the Landweber iteration with calculated ΔE_0 ('iteration') or by shell fit. Both results are in good agreement. Furthermore, they are in good agreement with the results obtained by keeping ΔE_0 constant during the Landweber iteration (Table 1, #6).

4. Application of Landweber's iteration to curium(III) hydrate

The coordination environment of the hydrated Cm^{3+} ion was recently investigated by Cm L_3 EXAFS and high-energy X-ray scattering (Skanthakumar *et al.*, 2007). It was found that the Cm^{3+} ion is surrounded by nine coordinating water molecules at two different Cm–O distances. The EXAFS spectrum was fitted by six oxygen atoms at 2.47 Å and three oxygen atoms at 2.63 Å, while maintaining the coordination numbers fixed to stabilize the shell fit (Skanthakumar *et al.*, 2007).

In order to test our full Landweber approach (including the procedure for determining ΔE_0) for deriving the RPDF of a real world spectrum, the authors of Skanthakumar *et al.* (2007) kindly provided their experimental Cm^{3+} hydrate spectrum [Fig. 6(a), #1].

Table 4

Summary of the structural parameters for Cm(III) hydrate and a theoretical example gained by the Landweber iteration and the shell fit, the theoretical (ν_{theor}) and L-curve (ν_{curv}) defined stopping parameters in the case of the Landweber iteration.

Example	$C_{\text{noise}} \times 10^4$	N	r (Å)	$\sigma^2 \times 10^3$ (Å ²)	ν_{theor}	ν_{curv}	ΔE_0 (eV)
Cm(III) hydrate	–	6.0 (6)	2.469 (4)	6.0 (3)	–	900	6.42
(Landweber iteration)	–	3.1 (7)	2.61 (2)	10 (2)	–	–	–
Cm(III) hydrate	–	6†	2.464 (1)	5.8 (2)	–	–	6.51 (4)
(Shell fit)	–	3†	2.612 (4)	9.5 (8)	–	–	–
Theoretical example	5	6.0 (2)	2.464 (1)	5.6 (1)	1709	1922	6.51†
(Landweber iteration)	–	2.9 (2)	2.614 (6)	8.7 (5)	–	–	–

† Fixed structural parameter. Standard deviations of the parameter are given in parentheses. In the case of the shell fit, the standard deviations were calculated by using the software EXAFSPAK (George & Pickering, 1995).

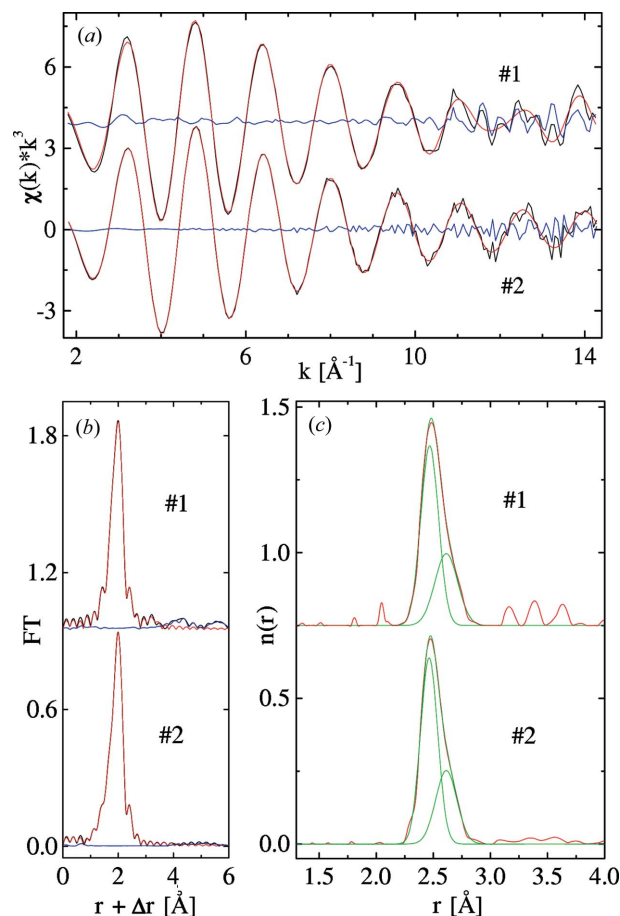


Figure 6

(#1) Experimental data of Cm(III) hydrate. (#2) Theoretical example. Data (black), result of the Landweber iteration (red), residual between data and result of Landweber iteration (blue). (a) EXAFS spectra, (b) corresponding Fourier transforms, (c) RPDFs. Decomposition of the RPDFs into two Gaussians and the sum of the two Gaussians (green).

For the calculation of the matrix A an r -interval of 1.3–4.0 Å with a step size of $\Delta r = 0.002$ Å is used. To determine ΔE_0 , the method described in §2.4 is applied and yields $\Delta E_0 = 6.42$ eV at $\nu_{\text{curv}} \simeq 900$ (Table 4). The determined RPDF shows an asymmetry at higher r -distances [Fig. 6(c), #1]. The small features at 3.1–3.8 Å in the RPDF [Fig. 6(c), #1] may arise from reproduction of small multiple-scattering contributions by the Cm–O functions or other sources. The determined asymmetric RPDF is only properly reproduced when two Gaussians are considered in equation (7) [Fig. 6(c), #1]. The

resulting structural parameters for the two Cm–O shells are within the standard deviations in full agreement with those gained by a shell fit of the Cm(III) hydrate spectrum (Table 4). The coordination numbers of the two Cm–O shells were assumed to be 6 and 3 and were fixed to stabilize the shell fit. Note that in the case of the Landweber iteration the RPDF is calculated without such constraints and assumptions contrary to the shell fit.

In the following we tested the ability of the Landweber iteration in resolving these two overlapping Cm–O shells by constructing a theoretical model. Both the model RPDF and χ were constructed using the structural parameters gained from the shell fit of the Cm(III) hydrate spectrum (Table 4) and the procedure discussed in §3. To the unweighted spectrum χ , we added noise C_{noise} (Table 4) similar to the noise amplitude of the experimental spectrum of Cm(III) hydrate [compare #1 and #2 in Fig. 6(a)]. The optimum number of iterations, $\nu_{\text{curv}} = 1922$, is near the theoretical optimum number of iterations of $\nu_{\text{theor}} = 1709$ (Table 4). For Cm(III) hydrate, ν_{curv} is much higher than for the theoretical examples discussed in §3, which were analyzed in the smaller r -interval of 2–3 Å. The higher ν_{curv} can be explained by the decrease of the convergence parameter α owing to the increasing norm $\|A^*A\|$ (see §2.1) in the case of the larger investigated r -interval of 1.3–4.0 Å.

The resulting RPDF [Fig. 6(c), #2] reproduces the noise-contaminated EXAFS spectrum [Fig. 6(a), #2] within the limits of the artificially added noise. Owing to the spatially distinct two oxygen shells, the RPDF shows an asymmetry at higher r -distances which is not visible in the corresponding Fourier transform [compare Figs. 6(b) and 6(c), #2], similar to the experimental data [compare Figs. 6(b) and 6(c), #1]. For the calculation of the structural parameters, the RPDF is reconstructed with two Gaussians according to equation (7). The resulting structural parameters (Table 4, theoretical example) are in good accordance with those taken for the construction of the theoretical RPDF (Table 4, shell fit), hence there is strong confidence in the correct calculation of the RPDF by the Landweber iteration in the case of the experimental Cm(III) hydrate spectrum. The structural parameter for Cm(III) hydrate, gained by the Landweber iteration and the shell fit (Table 4), agrees favorably with the results published by Skanthakumar *et al.* (2007) within the bounds of the errors in the determination of EXAFS structural parameters.

5. Conclusions

The analysis of model spectra with artificial noise, as well as of an experimental EXAFS spectrum of Cm(III) hydrate, demonstrates that the Landweber iteration approach is well suited to solving the EXAFS integral equation, even if the spectra contain experimental error. The robustness in relation to the error in the data represents the main advantage of this method.

All variables used in the iteration approach [equation (12)] have a well defined physical meaning. The determined RPDF $n(r)$ is the density of coordination numbers, the key trans-

formation with the matrix A^* is a windowed and phase-corrected Fourier transform of the spectrum, and the acceleration term $(\chi - An_{\nu})$ is the difference spectrum between the original spectrum χ and the last iteration spectrum An_{ν} . Convergence and stopping parameters are uniquely defined by the matrix A and the L-curve concept.

In the presented approach, the threshold energy shift ΔE_0 is defined by the iteration procedure itself, without recourse to fit-calculations or models.

The forthcoming investigations focus on the expansion of the stable Landweber iteration with the aim of considering more than one type of backscattering atoms and multiple-scattering effects for the inversion of the EXAFS equation.

We would like to thank the authors S. Skanthakumar, M. R. Antonio, R. E. Wilson and L. Soderholm for supplying the X-ray absorption spectrum of Cm(III) hydrate. We also thank F. Bridges (Department of Physics, University of California Santa Cruz, USA) and M. Kunicke (Forschungszentrum Dresden-Rossendorf, Germany) for fruitful discussions and suggestions. AR was supported through the German Science Foundation (DFG) under Contract RO 2254/3-1.

References

- Ageev, A. L., Korshunov, M. E., Reich, T. Y., Reich, T. & Moll, H. (2007). *J. Inv. Ill-Posed Problems*, **15**, 767–783.
- Ankudinov, A. L., Ravel, B., Rehr, J. J. & Conradson, S. D. (1998). *Phys. Rev. B*, **58**, 7565–7576.
- Babanov, Y. A., Kamensky, I. Y., Hazemann, J. L., Calzavara, Y. & Raoux, D. (2007). *Nucl. Instrum. Methods Phys. Res. A*, **575**, 155–158.
- Babanov, Y. A., Vasin, V. V., Ageev, A. L. & Ershov, N. V. (1981). *Phys. Status Solidi B*, **105**, 747–757.
- Bunker, G. (2009). Private communication.
- Bunker, G., Dimakis, N. & Khelashvili, G. (2005). *J. Synchrotron Rad.* **12**, 53–56.
- Crozier, E. D., Rehr, J. J. & Ingalls, R. (1988). *X-ray Absorption*. New York: John Wiley and Sons.
- Dalba, G. & Fornasini, P. (1997). *J. Synchrotron Rad.* **4**, 243–255.
- Elfving, T. & Nikazad, T. (2007). *Inv. Probl.* **23**, 1417–1432.
- Ershov, N. V., Ageev, A. L., Vasin, V. V. & Babanov, Y. A. (1981). *Phys. Status Solidi B*, **108**, 103–111.
- George, G. N. & Pickering, I. J. (1995). *EXAFSPAK: A Suite of Computer Programs for Analysis of X-ray Absorption Spectra*. Stanford Synchrotron Radiation Laboratory, Stanford, CA, USA.
- Hadamard, J. (1932). *Le Problème de Cauchy et les Équations aux Dérivées Partielles Linéaires Hyperboliques*. Paris: Hermann.
- Hansen, P. C. (1992). *SIAM Rev.* **34**, 561–580.
- Hansen, P. C. (2001). *Inverse Problems in Electrocardiology*. Southampton: WIT Press.
- Hansen, P. C. & O'Leary, D. P. (1993). *SIAM J. Sci. Comput.* **14**, 1487–1503.
- Khelashvili, G. & Bunker, G. (1999). *J. Synchrotron Rad.* **6**, 271–273.
- Kirsch, A. (1996). *An Introduction to the Mathematical Theory of Inverse Problems*. New York: Springer.
- Kunicke, M., Kamensky, I. Y., Babanov, Y. A. & Funke, H. (2005). *Phys. Scr.* **T115**, 237–239.
- Landweber, L. (1951). *Am. J. Math. Manag. Technol.* **73**, 615–624.
- Latham, G. A. (1998). *Inv. Probl.* **14**, 1527–1537.
- Lee, J. M. & Yang, D. S. (2006). *XAFS 13*, pp. 138–140. Stanford, USA.
- Lee, P. A. & Pendry, J. B. (1975). *Phys. Rev. B*, **11**, 2795–2811.

- Louis, A. K. (1989). *Inverse und Schlecht Gestellte Probleme*. Stuttgart: Teubner.
- Skanthakumar, S., Antonio, M. R., Wilson, R. E. & Soderholm, L. (2007). *Inorg. Chem.* **46**, 3485–3491.
- Stern, E. A. (1974). *Phys. Rev. B.* **10**, 3027–3037.
- Teo, B. K. (1986). *EXAFS: Basic Principles and Data Analysis*. Berlin/Heidelberg/New York/Tokyo: Springer.
- Tikhonov, A. N. & Arsenin, V. Y. (1981). *Solution of Ill-Posed Problems*. New York: John Wiley and Sons.
- Yamaguchi, K., Ito, Y., Mukoyama, T., Takahashi, M. & Emura, S. (1999). *J. Phys. B.* **32**, 1393–1408.
- Yang, D. S. & Bunker, G. (1996). *Phys. Rev. B.* **54**, 3169–3172.
- Yang, D. S. & Joo, S. K. (1998). *Solid State Commun.* **105**, 595–599.